Optical diffractometry of highly anisotropic holographic gratings formed by liquid crystal and polymer phase separation

Hiroshi Kakiuchida,* Masato Tazawa, and Kazuki Yoshimura
Materials Research Institute for Sustainable Development, National Institute of Advanced Industrial Science and Technology, 2266-98 Anagahora, Shimoshidami, Moriyama-ku, Nagoya, Aichi 463-8560, Japan

Akifumi Ogiwara
Department of Electronics Engineering, Kobe City College of Technology, 8-3 Gakuen-higashimachi, Nishi-ku, Kobe, Hyogo 651-2194, Japan
(Received 12 July 2012; published 12 December 2012)

Optical diffractometry is proposed as a practical method of quantitatively analyzing the microscopic structural origins of a wide range of highly efficient and linearly polarized optical diffraction grating produced from holographic polymer-dispersed liquid crystal. The structure is organized by a spatially periodical distribution of submicrometer-scale liquid crystal (LC) droplets in a polymer matrix. Six independent Bragg diffraction spectra were obtained at two orthogonal polarization states at temperatures below, at, and above the nematic-to-isotropic phase transition point. These spectra were simultaneously analyzed by employing anisotropic diffraction theory under the restraint of a simple and widely useful structural model constructed on the basis of the previously reported microscopic observations. The refractive indices of spatially periodic LC- and polymer-rich phases were analyzed using Cauchy's equation as a function of optical wavelength. The present diffractometry was demonstrated for a variety of holographic structures, and the structural parameters were discussed such as the filling ratio of LC droplets to polymer matrix, the orientational order in the droplets, and the thermo-optic properties in the LC droplets. Furthermore, the higher order Bragg diffractions were measured and discussed. The proposed method was examined in consistency by comparisons with polarizing optical microscopy and scanning electron microscopy.

DOI: 10.1103/PhysRevE.86.061701 PACS number(s): 61.30.Pq, 61.30.Gd, 64.70.M−, 42.40.Eq

I. INTRODUCTION

A holographic polymer-dispersed liquid crystal (HPDLC) consists of both liquid crystal (LC) and polymer phases, as schematically shown in Fig. 1, and its refractive index is spatially periodically modulated. It can be an anisotropic optical Bragg grating; that is, it can efficiently diffract linearly polarized light parallel or perpendicular to the grating vector. HPDLCs have a great promise for electrically, thermally, and optically switchable holographic devices. Various advanced applications have been proposed, such as optically switchable Bragg reflectors doped with azobenzene dye [1], electrically tunable photonic crystal structures [2,3], and thermally responsive band pass filters [4,5]. The fundamental properties of HPDLCs, that is, the amplitude and anisotropy of refractive-index modulation and their responsiveness to extrinsic stimuli, are indispensable for promoting the performance for such varied applications. Sarkar *et al.* investigated the relationship between the phase-separated morphology and functionality of photoreactive monomers in order to encourage diffraction switchability [6]. Jeong reported the suppression of the so-called anchoring effect in LC droplets with a siloxane polymer, which enhances LC molecular rotational mobility [7]. Wu *et al.* demonstrated the improved electrical switchability of the diffraction intensity by employing an additional compound with high dielectric anisotropy [8].

The spatially periodic structure of HPDLCs is usually created by using interferometric photoirradiation that induces polymerization and subsequent phase separation in a mixture of a photoreactive monomer and a LC. During the exposure, the monomer is polymerized more efficiently in the areas of the mixture that receive more intense irradiation, while LC molecules are pushed out into the areas that receive less irradiation. Thus, LC molecules are considered to be spontaneously oriented along the grating vector to form a LC-rich phase. The internal structures such as phase-separated morphology and LC molecular orientation have been examined extensively by using several measurement methods, with scanning electron microscopy (SEM), polarizing optical microscopy (POM), and optical diffractometry being the most popular. SEM and POM are well established, and they provide direct images of the periodic structure of HPDLCs. However, the samples for SEM must be sectioned, which prevents LC droplets from being observed directly, and the image resolution of POM is limited for submicrometer-scale structures, whereas the microscopic anisotropy can be detected. Although optical diffractometry cannot provide immediate microscopic images, it allows for quantitative analysis of the structures, such as the grating pitch, and the amplitude and anisotropy of the refractive-index modulation. Furthermore, structural information such as the morphology and distribution of LC droplets and the orientational order of LC molecules in the droplets can be obtained on a scale smaller than optical wavelengths if an appropriate structural model is assumed and spectroscopic data are gathered sufficiently with regard to quantity and quality.

Many measurement and analysis methods to obtain microscopic information of HPDLCs have been proposed and improved by Kogelnik and other groups, as detailed below. For thick optical gratings, strong diffraction appears selectively

*Corresponding author: h.kakiuchida@aist.go.jp

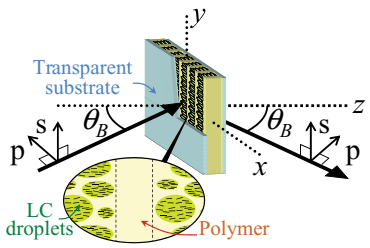

FIG. 1. (Color online) Scheme illustrating the internal structure and Bragg diffraction of HPDLC.

in the case that the relationship between incident angle and wavelength satisfies the Bragg's condition, and then the diffraction intensity provides the amplitude of microscopic refractive-index modulation in gratings. In practice, finite-thick gratings produce diffraction curve with certain width around the Bragg peak as a function of the deviation in incident angle (wavelength) from the Bragg's one, and the structural information in the optical gratings such as the amplitude of refractive-index modulation, pitch, and thickness can be obtained by measurement and analysis of the curve shape around the Bragg peak. Thus, the examination of diffraction intensity at or around a set of incident angle and wavelength satisfying the Bragg's condition can provide a solution for the amplitude of the refractive-index modulation. However, to solely determine the value, diffractions at plural sets of Bragg angles and wavelengths should be examined, because diffraction intensity periodically changes against the amplitude of refractive-index modulation. Furthermore, the analysis of diffraction properties at the Bragg angles (wavelengths) in wide range is effective to clarify the microscopic optical anisotropy in HPDLCs, since the results at the larger (longer) Bragg angles (wavelengths) provide the information in direction along grating thickness, as shown by the z axis in Fig. 1, while those at the smaller (shorter) Bragg's angles (wavelengths) provide the information perpendicular to direction along grating thickness, as shown by the x-y plane in Fig. 1.

Bragg diffraction can be produced in HPDLCs from the periodic spatial modulation of the refractive index due to nonuniform distributions of LC droplets in the polymer matrix or, in other words, due to the LC- and polymer-rich periodic phases. The strong polarization state in the diffraction is considered to arise from the highly ordered orientation of LC molecules in the droplets. The morphology and distribution of the droplets strongly influence the orientational order of the LC molecules, particularly when the droplet size is several tens or hundreds of nanometers [9,10]. LC molecular orientation in the droplets was found to be unidirectional along the grating vector, and the reason for this orientation is regarded as the surface anchoring effect or, in other words, the chemical interactions of the LC molecules with the polymer surface that surrounds the droplets and that is distributed perpendicular to the grating vector.

The relationship between the diffraction properties and the internal structure of HPDLCs has been quantitatively investigated based on diffraction theory. Kogelnik proposed the coupled wave theory for analysis of thick holographic gratings [11]. Montemezzani *et al.* generalized the coupled wave theory to describe various optical anisotropic gratings such as organic crystals, ordered polymers, and aligned LCs [12]. Butler *et al.* and Holmes *et al.* quantitatively discussed the orientational order of LC molecules by analyzing the anisotropic diffraction spectrum [13–15]. Jazbinšek *et al.* reported on the relationship between the grating pitch and the diffraction anisotropy [16]. Olenik *et al.* analyzed the relationship between the LC droplet morphology and the LC molecular birefringence, and they indicated that ellipsoidal droplets induce ordered alignment of LC molecules and, consequently, polarized diffraction [17,18]. Lucchetta *et al.* determined accurately the small anisotropy in HPDLC, based on two-wave theory in comparison with that of Kogelnik [19]. Heretofore, the microscopic origins of highly polarized diffraction produced from HPDLCs have been analyzed by diffraction spectroscopy at a particular polarization azimuth, as mentioned before.

In the present study, an advanced diffraction analysis of highly anisotropic HPDLC gratings is proposed, in which six independent Bragg diffraction spectra measured in two orthogonal polarization states at temperatures below, at, and above the nematic-to-isotropic phase transition point (T_{NI}) were consistently analyzed all at once. The analysis was based on anisotropic diffraction theory employing a widely useful structural model constructed on the basis of the previous reports, such as LC orientational order, phase separation degree, and thermo-optic properties. Then, the refractive indices of the spatially periodic LC- and polymer-rich phases were determined as a function of optical wavelength, which is valid for the accurate design of diffractive devices. By strict fitting calculations, the wavelength dispersion from visible to near-infrared wavelengths was determined separately in the refractive indices for LC- and polymer-rich phases. The effectiveness of the present approach was verified by comparison with polarizing optical microscopy and SEM.

II. EXPERIMENTS

A. Sample preparation

HPDLCs were prepared from mixtures of a LC, a photopolymerizable monomer, a photoinitiator, and a coinitiator in various proportions (Table I). Two types of nematic LC materials with different wavelength dispersions and temperature dependencies in refractive indices were used (BL024 and K15, Merck Corp.). 2-Hydroxy-3-phenoxypropyl acrylate, 2-hydroxyethyl methacrylate, and dimethylol tricyclodecane diacrylate (Kyoeisha Chemical Co., Ltd.) were mixed as the prepolymer. The LC material and the prepolymer were combined, and then the photoinitiator dibromofluorescein and the coinitiator N-phenylglycine (Tokyo Chemical Industry Co., Ltd.) were added to the mixture. Samples I–III were prepared using constant weight ratios of the prepolymers and BL024, of which T_{NI} is 81 °C, in order to examine the influence of the LC droplet size and distribution on the diffraction properties. Samples IV–VI were prepared by adding different weight ratios of K15, of which T_{NI} is 35 °C, to the mixture in order to examine the effect of the filling ratio of LC droplets in the periodic structure on the diffraction properties.

TABLE I. Compositions and fabrication conditions of HPDLC samples.

Sample	LC (wt%)		Photopolymerizable monomer mixture (wt%) (1) AH600	(2) DCPA	(3) HO	(1) + (2) + (3)	Coinitiator NPG (wt%)	Photoinitiator DBF (wt%)	Exposure temperature (°C)	Grating Pitch (μm)
I	BL024	**25**	60	10	5	**75**	0.1[a]	0.1[a]	30	**0.71**
II	BL024	**25**	60	10	5	**75**	0.1[a]	0.1[a]	55	**0.71**
III	BL024	**25**	60	10	5	**75**	0.1[a]	0.1[a]	80	**0.71**
IV	K15	**40**	45	10	5	**60**	0.1[a]	0.1[a]	40	**1.03**
V	K15	**45**	40	10	5	**55**	0.1[a]	0.1[a]	40	**1.03**
VI	K15	**50**	35	10	5	**50**	0.1[a]	0.1[a]	40	**1.03**

[a]Additional content.

The mixtures were placed in a 10-μm gap between a pair of transparent glass cells ($25 \times 20 \times 1$ mm). The width of the gap was carefully determined by examining multiple interference spectra. The cells were mounted on a holographic exposure system that was equipped with a thermoregulator to control the sample cell temperature during the exposure. (Sub)micrometer-scale periodic structures were formed by photopolymerization during a 5-min holographic exposure and subsequent phase separation of the LC- and polymer-rich components. The light source was a single-mode Nd:YVO_4 laser oscillated at a wavelength of 532 nm. The beam was collimated, expanded, linearly polarized, and split into two beams to produce interferometric irradiation onto the sample cell. The spatial intensity modulation in the interference was maintained at an amplitude of 10 mW/cm^2, with a pitch of 0.71 μm for samples I–III and 1.03 μm for samples IV–VI. Following the holographic exposure, any remaining monomer was completely polymerized by homogeneous irradiation with an ultraviolet lamp at an intensity of 0.8 mW/cm^2.

B. Measurements

Bragg diffraction intensities at wavelengths from 0.4 to 2.5 μm were measured through changes in the angles of incidence and diffraction using a spectrophotometer (U4100, Hitachi High-Technologies Corp.) with a built-in thermoregulator for control of sample temperature. The diffracted light was detected at the incident and diffracted angles from 20° to 50° in air. In particular, when the diffracted intensity was detected at long wavelengths or at large angles of incidence and diffraction, the sample cells were sandwiched between a pair of isosceles right triangular optical prisms with refractive index-matching oil between them. The incident light was collimated at a divergence angle less than 0.35°. The resolution was 2 nm for wavelengths below 0.85 μm and 16 nm for wavelengths above 0.85 μm. p- and s-polarization states were set by the azimuths of a polarizer with an extinction ratio of less than 5×10^{-6}. The diffraction efficiency was obtained by normalizing the diffracted intensity by using the transmitted intensity at 0° in angles of incidence and transmission, where the transmittance change at surfaces of specimen substrates against angle of incidence based on Fresnel equations was considered.

The refractive indices for the LC material and polymer mixture were determined in advance as a function of wavelength using a three-term Cauchy's equation and were then used as fundamental data for the fitting calculations. Refractive indices for extraordinary and ordinary rays of the LC at a temperature of T_{NI}, n_e and n_o, respectively, were obtained from the optical transmittance spectra. The LC material was injected into gaps of 5 and 15 μm in transparent cells with rubbing-treated glass surfaces for orienting the LC molecules. The transmittance of the cells mounted in the optical path between a pair of polarizers in parallel and crossed Nicol arrangements was measured at temperatures below, at, and above T_{NI}. The refractive indices of the LC materials at temperatures at and above T_{NI}, n_i, and of the polymer, n_{ply}, were measured by a spectroscopic ellipsometer (M2000, J. A. Woolam).

The microscopic phase-separated structures were observed by POM (Optiphot-2 with polarizer plates, Nikon Corp.) and SEM (S-4300, Hitachi High-Technologies Corp.) in order to establish and verify the structural parameters that were employed as the restraints in the fitting calculations of the diffraction data. The anisotropy in the microstructure was observed by POM in a crossed Nicol state. The submicrometer-scale morphology, which influences optical homogeneity and LC molecular orientation, was observed by SEM. Although LC droplets could not be directly observed with our equipment, the droplet shape and distribution were recognized as traces by voids in the polymer matrix after the LC molecules were rinsed away with methanol.

III. MODELING OF PERIODIC STRUCTURE

Some structural models have been proposed being focused on particular structures in HPDLCs [14,15]. For example, Holmes *et al.* constructed the model where LC was aggregated as anisotropic droplets to form LC-rich phase, whereas it is trapped as a dissolved state to form a polymer-rich phase. However, several practical HPDLCs were reported to possess LC droplets not only in the LC-rich phase but also in the polymer-rich one, and their model insufficiently expresses such practical structures.

In the present study, a simple but widely useful structural model was employed, as shown in Fig. 2, by classifying several microscopic structures previously reported. The features were summarized as follows. (i) LC molecules aggregate to form submicrometer-scale droplets [17,20]. (ii) The LC droplets are distributed to form a LC-rich phase, and the droplets could also be present in the polymer-rich

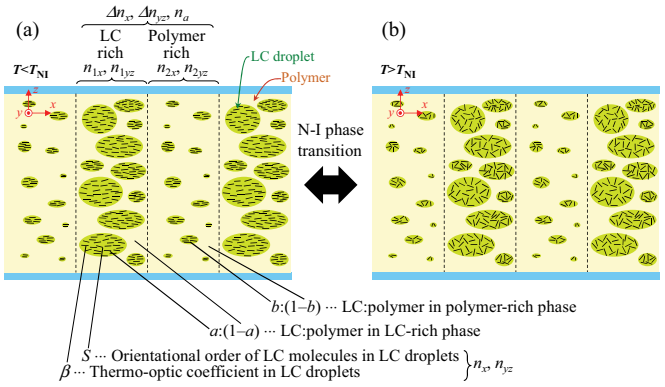

FIG. 2. (Color online) The present structural model of periodic structure in HPDLCs constructed based on (i)–(iv) in Sec. III. Panels (a) and (b) are at temperatures below and above T_{NI}, respectively. The structural parameters a, b, β, and S are expressed in Eqs. (6)–(11). Note that the x, y, and z directions correspond to those in Fig. 1

phase, depending on fabrication conditions, while the polymer matrix could intrude into the LC-rich phase. [3,8,16,21,22]. (iii) The optical anisotropy of the periodic structure is uniaxial along the grating vector at temperatures below T_{NI} [23]. (iv) The present examination of diffraction polarization, as detailed below, suggests that the optical anisotropy does not disappear completely above T_{NI} in some of the samples. The microscopic origin of (iv) is unresolved yet in the present study but is speculated to result from LC molecular orientation in the droplets, of which idea is referred to the previous reports, that is, the dependence of nematic-to-isotropic phase transition temperature on LC content in LC-polymer composites [22,24–26]. Based on these points, a widely useful structural model was established and used as the restraint in an analysis of a practical HPDLC structure by using six diffraction spectra that were measured under independent conditions.

The physical properties of the LC- and polymer-rich phases, which form a one-dimensional periodic structure, were analyzed by the amplitude and anisotropy of the refractive-index spatial modulation as a function of wavelength and temperature. The Bragg diffraction by the transmissive one-dimensional holographic grating with a grating vector along the x axis was considered, as schematically shown in Fig. 1. The diffracted light obeys Bragg's condition, $\lambda_B = 2\Lambda \sin\theta_B$, where θ_B and $-\theta_B$ are the angles of incidence and diffraction, respectively, λ_B is the Bragg wavelength, and Λ is the pitch of the grating. The diffraction spectrum was analyzed individually for two orthogonal linear polarizations, where p polarization is the component in the plane that includes the incident and diffracted rays and s polarization is perpendicular to the plane. According to Butler *et al.* [13,14], the diffraction efficiency by anisotropic optical gratings with sinusoidally modulated refractive index can be described for the p- and s-polarized components, as a function of the Bragg wavelength, as follows:

$$\eta_p = \sin^2\left(\frac{\pi d}{2n_a\Lambda\lambda_B}\frac{4n_a^2\Lambda^2\Delta n_x - \lambda_B^2(\Delta n_x + \Delta n_z)}{\left(4n_a^2\Lambda^2 - \lambda_B^2\right)^{1/2}}\right) \quad \text{and} \tag{1}$$

$$\eta_s = \sin^2\left(\frac{\pi d}{2n_a\Lambda\lambda_B}\frac{4n_a^2\Lambda^2\Delta n_y}{\left(4n_a^2\Lambda^2 - \lambda_B^2\right)^{1/2}}\right), \tag{2}$$

respectively, where d is the thickness and n_a is the spatially averaged refractive index in the HPDLC. The analyses of the diffraction spectra for the p- and s-polarized components measured at temperatures below and above T_{NI} provide the amplitudes of sinusoidal refractive-index modulation at x, y, and z axes, Δn_x, Δn_y, and Δn_z, respectively, and spatially average refractive index, n_a. Consequently, these analyses can be used to characterize the microscopic structure of the HPDLC.

To connect the refractive indices with the internal structure in HPDLCs, a structural model was constructed based on the aforementioned structural information (i)–(iv) (see Fig. 2). According to (ii), the boundary of periodic structure of HPDLC gratings is not necessarily apparent, but the polymer and LC are able to intrude into each other to form the respective rich phases. These complex phases have uniaxial anisotropy along

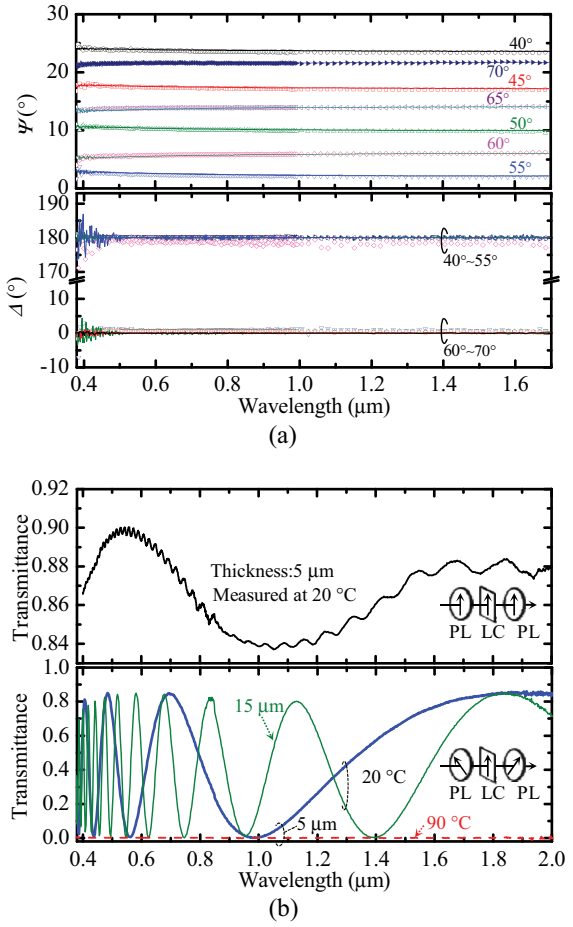

FIG. 3. (Color online) The ellipsometric parameters and transmittance spectra used to determine the respective refractive indices of LC material and polymer. (a) Ellipsometric data for the polymer as a function of wavelength at angles of incidence from 40° to 70°. (b) Polarized transmittance spectra of the LC material BL024 between a pair of glass substrates. The arrangements of polarizers and sample cell in the measurement setup are shown in the graphs.

the x axis, as stated in (iii), so that the refractive indices, n_{1x} and n_{1yz}, are set for the optical polarizations parallel and perpendicular to the x axis in the LC-rich phase, respectively, and n_{2x} and n_{2yz} are set in the same way in the polymer-rich phase. These parameters are used to express the amplitudes of the refractive-index modulations and the spatially averaged refractive index:

$$\Delta n_x = |n_{1x} - n_{2x}|/2, \tag{3}$$

$$\Delta n_y = \Delta n_z = |n_{1yz} - n_{2yz}|/2, \quad \text{and} \tag{4}$$

$$n_a = \{(n_{1x} + 2n_{1yz})/3 + (n_{2x} + 2n_{2yz})/3\}/2. \tag{5}$$

In the present study, the refractive indices in the HPDLCs are assumed to be additive, that is, the values of n_{1x}, n_{1yz}, n_{2x}, and n_{2yz} are regarded as linear functions of the refractive index of the polymer, n_{ply}, and of those of the LC material for the extraordinary and ordinary rays, n_e and n_o, respectively. As stated in (i), LC molecules are aggregated to form submicrometer-scale droplets and that the LC- and polymer-rich phases consist of the spatial modulation of the droplet distribution. On the other hand, according to (iii), the LC molecules in the droplets are considered to be uniaxially oriented along the x axis. Thus, the refractive indices in the LC droplets at temperatures below T_{NI} are expressed in terms of n_e and n_o as follows, for polarizations parallel and perpendicular to the x axis, respectively:

$$n_x = \{1 + \beta(T - T_0)\}\frac{(1 + 2S(T))n_e + 2(1 - S(T))n_o}{3} \quad \text{and} \tag{6}$$

$$n_{yz} = \{1 + \beta(T - T_0)\}\frac{(1 - S(T))n_e + (2 + S(T))n_o}{3}. \tag{7}$$

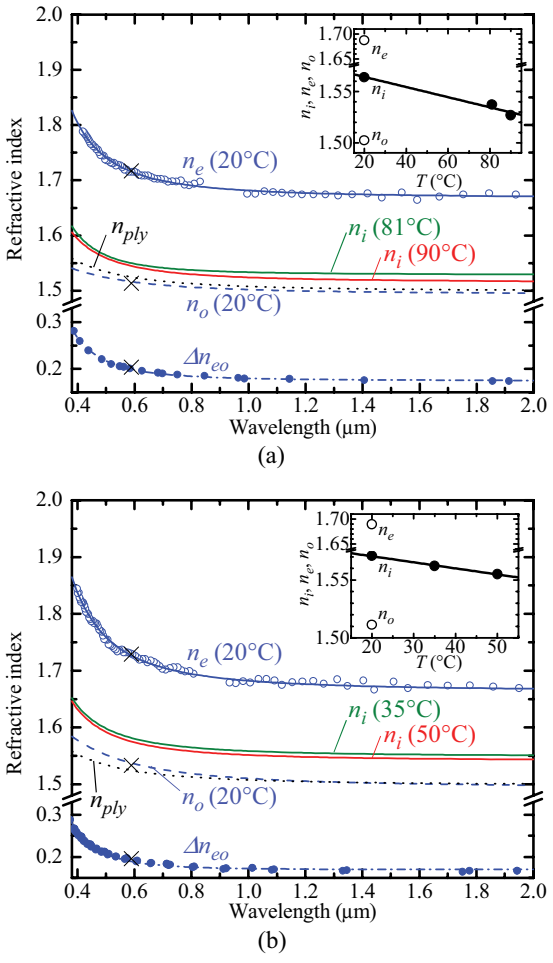

FIG. 4. (Color online) Refractive indices for the LC material at three different temperatures and for the polymer as a function of wavelength. The refractive indices of the extraordinary and ordinary rays, n_e and n_o, below T_{NI}, and that of isotropic phase, n_i, at and above T_{NI}, for LC materials (a) BL024 and (b) K15, and that of the polymer, n_{ply}. The blue solid circles and broken curves correspond to the measurement and fitting of $\Delta n_{eo}(=n_e - n_o)$. The insets are the temperature dependence of the refractive indices of n_e, n_o (open circles), and n_i (solid circles), which were averaged in the present wavelength range, and the solid lines are the fittings for n_i. The literature values of n_e and n_o are shown as crosses [29–31].

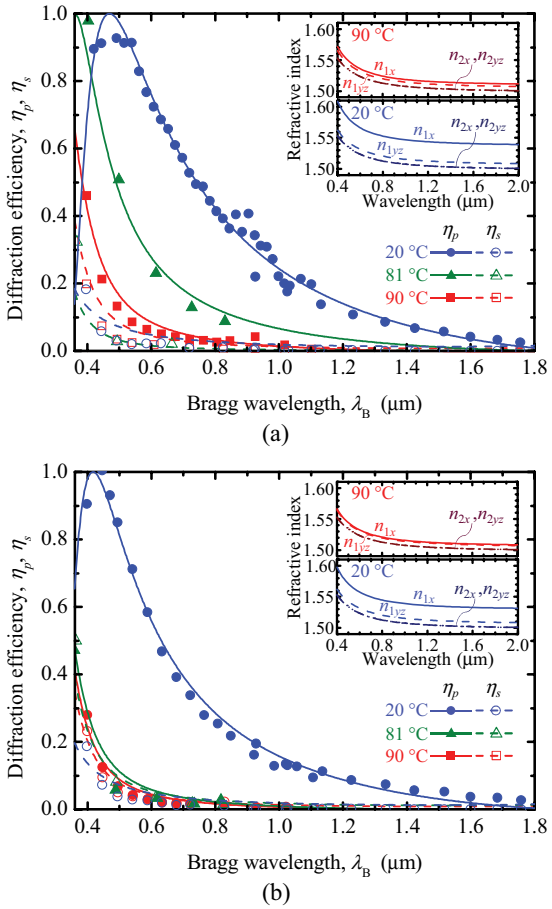

FIG. 5. (Color online) Diffraction spectra of (a) sample I and (b) sample III, which were prepared at exposure temperatures of 30 °C and 80 °C, in two orthogonal polarization states at temperatures below, at, and above T_{NI}. The solid and open symbols indicate p- and s-polarization states, respectively. The blue circles, green triangles, and red rectangles indicate the data obtained at 20 °C, 81 °C, and 90 °C, respectively. The solid and broken curves are the fittings. Insets show the analyzed refractive indices of the LC- and polymer-rich phases at 20 °C and 90 °C, where n_{1x}, n_{1yz}, n_{2x}, and n_{2yz} are explained in the text.

The birefringence of the aggregated LC molecules is expressed by orientational order parameter, $S(T)$, as a function of temperature, T, which is theoretically expressed by Legendre's complete elliptic integral of the first kind [27,28]. In practice, in the present study, S is approximately regarded as a linear function varying from zero to one with birefringence in the LC droplets, as expressed in Eqs. (6) and (7). β is introduced as the thermo-optic coefficient to account for thermal change in the average refractive index of LC materials. Because the optical anisotropy of LC aggregation confined as the droplets is most likely different from that in loose states by considering (iv), the values of n_e and n_o pre-examined in the loose states are regarded inappropriate to be employed as constants in the fitting calculations. T_0 is the reference temperature adequately below T_{NI}, which was set at 20 °C in the present experiment. The boundaries between the LC- and polymer-rich phases in the periodic structure were found to be indistinct as stated in (ii), so that the parameters a and b ($0 \leqslant a \leqslant 1, 0 \leqslant b \leqslant 1$) are employed here as the filling ratios of the LC droplets in the respective phases. Then, the refractive indices of the LC-rich phase can be expressed by using n_x and n_{yz}, as well as n_{ply}, such that

$$n_{1x} = an_x + (1-a)n_{ply} \quad \text{and} \tag{8}$$

$$n_{1yz} = an_{yz} + (1-a)n_{ply} \tag{9}$$

for polarizations parallel and perpendicular to the x axis, respectively. In the same way, the refractive indices of the polymer-rich phase can be expressed as

$$n_{2x} = bn_x + (1-b)n_{ply} \quad \text{and} \tag{10}$$

$$n_{2yz} = bn_{yz} + (1-b)n_{ply} \tag{11}$$

for polarizations parallel and perpendicular to the x axis, respectively. It was found that the diffraction spectra may be polarized even at temperatures at and above T_{NI} for the samples from certain preparation conditions, which is shown and discussed in the later sections.

The p- and s-polarization components of the diffraction spectra at temperatures below, at, and above T_{NI} were individually measured, and these six spectra were simultaneously fitted to Eqs. (1) and (2) under the restraints imposed by Eqs. (3)–(11). Then, the wavelength dispersion of the refractive indices for the LC- and polymer-rich phases were obtained and the structural parameters a, b, β, and S were determined.

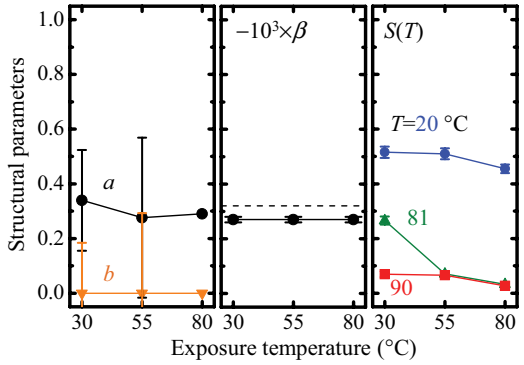

FIG. 6. (Color online) Structural parameters of HPDLCs as expressed in Eqs. (6)–(11) as functions of the exposure temperature, corresponding to samples I–III. Note that broken line in the graph of β corresponds to -0.32×10^{-3} (K^{-1}), estimated from the results in Fig. 4(a).

IV. RESULTS

A. Refractive indices of LC and polymer

The refractive indices of the polymer and the LC materials were determined in advance as a function of wavelength by spectroscopic ellipsometry or polarizing transmittance spectroscopy. These fundamental refractive indices were substituted in Eqs. (6)–(11) to determine the structural parameters, a, b, β, and S. The polymer film was singly formed in a 10-μm gap between two glass substrates using the same procedure as that described in Sec. II A. The refractive index of the polymer, n_{ply}, was determined by using a spectroscopic ellipsometer.

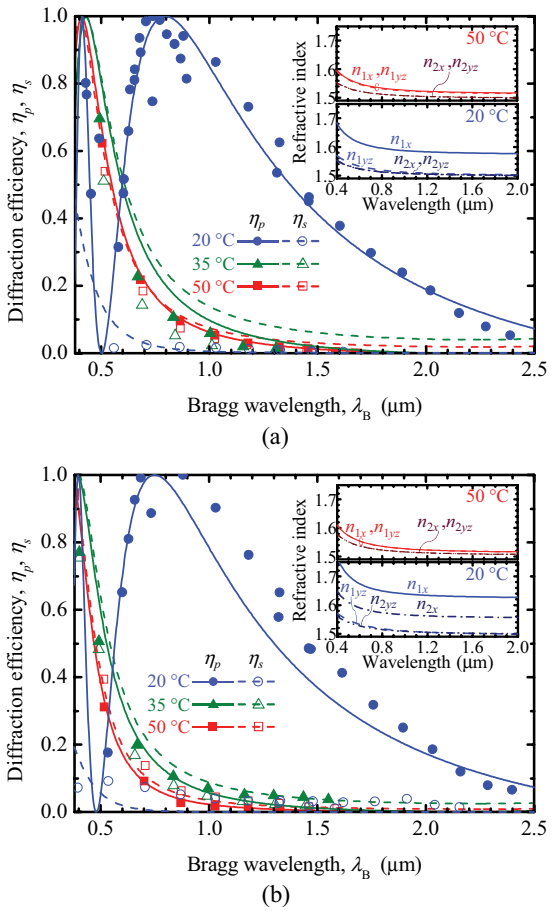

FIG. 7. (Color online) Diffraction spectra of (a) sample IV and (b) sample VI, which were prepared at different compositional ratios of LC, in two orthogonal polarizations at temperatures below, at, and above T_{NI}. The solid and open circles represent the data for p- and s-polarization states, respectively. The blue circles, green triangles, and red rectangles represent the data obtained at 20 °C, 35 °C, and 50 °C, respectively. The solid and broken curves are the fittings. Insets show the analyzed refractive indices of the LC- and polymer-rich phases at 20 °C and 50 °C, where n_{1x}, n_{1yz}, n_{2x}, and n_{2yz} are explained in the text.

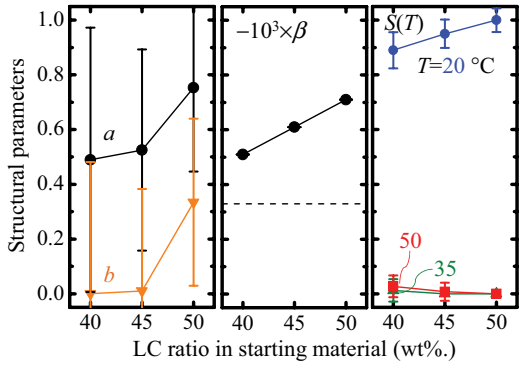

FIG. 8. (Color online) Structural parameters of HPDLCs as expressed in Eqs. (6)–(11) as functions of LC ratio in the starting material mixture, corresponding to samples IV–VI. Note that the broken line in the graph of β corresponds to -0.33×10^{-3} (K^{-1}), estimated from the results in Fig. 4(b).

Two ellipsometric parameters, ψ and Δ, were measured as a function of the wavelength at several angles of incidence, as shown in Fig. 3(a). The solid curves are the fittings and show that the measurements agree with the calculations based on three-term Cauchy's equation as

$$n_{ply}(\lambda) = 1.498\,4 + 0.009\,28\lambda^{-2} - 0.000\,09\lambda^{-4}, \quad (12)$$

where the optical wavelength unit is in micrometers.

The anisotropy of the present LC materials were confirmed at temperatures below, at, and above T_{NI}. Then, the refractive indices for the LC were determined in the nematic state below T_{NI}, n_e and n_o, and in isotropic states at and above T_{NI}, n_i. The LC material was injected into a 5- or 15-μm gap between a pair of glass substrates equipped with rubbing-treated polyimide thin layers to align the LC director along the x axis. The refractive indices of the LC materials, n_e and n_o, were obtained by polarized transmittance spectra. Figure 3(b) shows the spectra of BL024 mounted between two polarizers. The solid curve in the upper graph shows the transmittance when both the polarizer azimuths were set parallel to the x axis of the sample. The optical setups for the transmittance measurements are schematically shown in the graphs, where PL denotes the polarizer and LC denotes the LC cell. The arrows are the polarization azimuth and LC-oriented direction. The periodic change in the transmittance as a function wavelength was produced by multiple reflections in the layer of LC molecules oriented along the x axis between the glass substrates. The wavelength dispersion of the refractive index for the extraordinary ray, n_e, was determined from the peak and valley wavelengths of the transmittance. The lower graph in Fig. 3(b) shows the transmittance when the two polarizer azimuths were in a crossed Nicol state, that is, at –45° and 45° from the x axis, respectively. The solid curves correspond to the measurements at temperatures below T_{NI} and the broken curves correspond to those above T_{NI}. The blue (thick) and green (thin) solid curves are for the 5- and 15-μm-thick LC layers between the glass substrates at 20 °C, respectively. At temperatures below T_{NI}, the periodic variation with the wavelength indicates optical anisotropy arising from LC alignment. The birefringence, $(n_e - n_o)$, was estimated from the wavelengths of the peaks and valleys. By zero transmittance at all the wavelengths, as shown by the broken curve, LC molecules were confirmed to be in an isotropic state at temperatures above T_{NI}. The wavelength dispersion of the refractive index for the ordinary ray, n_o was obtained by the subtraction of $(n_e - n_o)$ from n_e. The wavelength dispersions of n_e and n_o for BL024 at 20 °C are expressed by Cauchy's equation

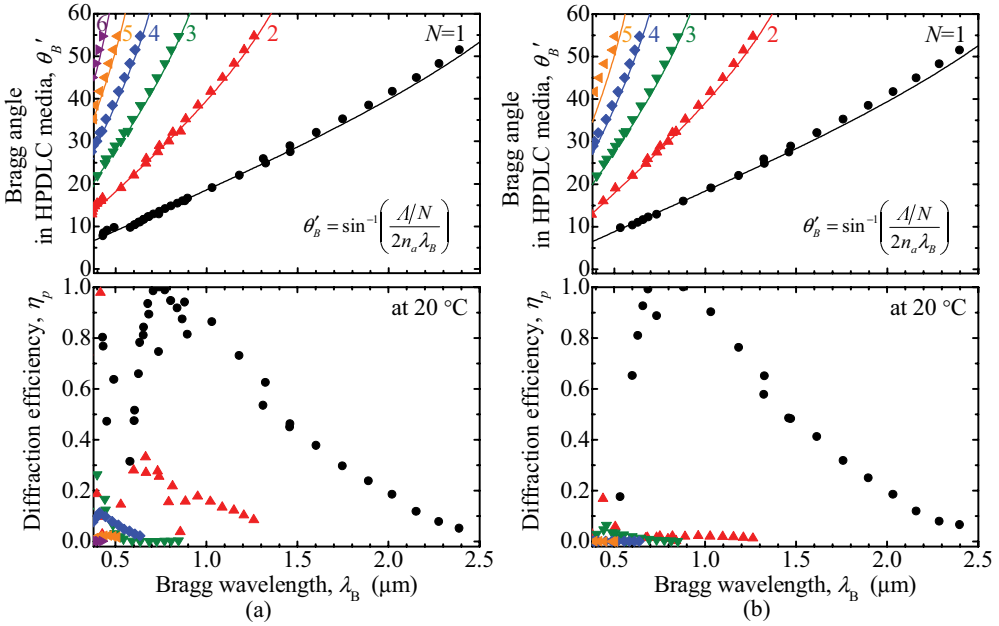

FIG. 9. (Color online) All the Bragg diffraction spectra detected in p polarization state at 20 °C for (a) sample IV and (b) sample VI. The upper graphs are the relationship between the Bragg angle and wavelength. The lower graphs are diffraction efficiency as a function of the Bragg wavelength. The data are grouped and numbered by N, as expressed by different symbols and colors. Solid curves for the respective N are drawn by modified Bragg formula, as stated in the graphs, where the detail is in the text.

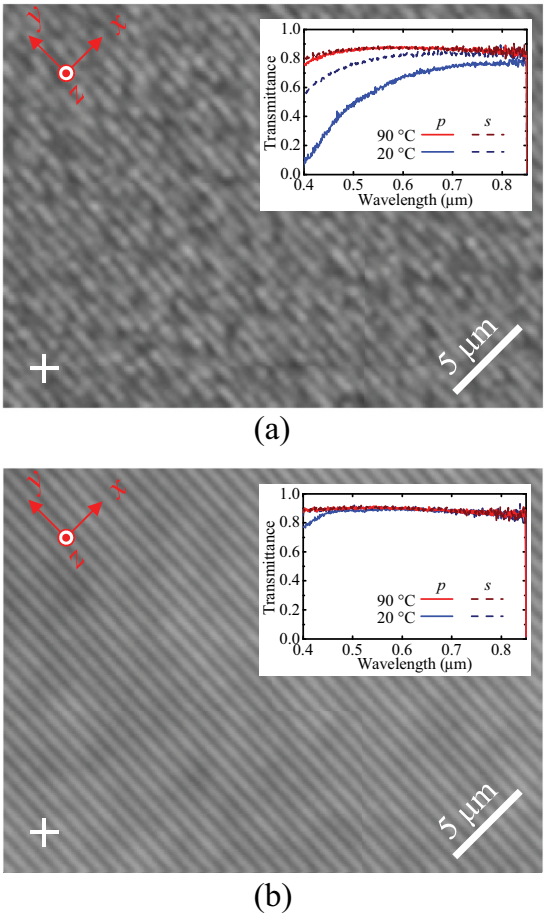

FIG. 10. (Color online) HPDLC transmission images of samples exposed at different temperatures, observed by POM in a crossed Nicol state at 20 °C: (a) sample I and (b) sample III, which were prepared at exposure temperatures of 30 °C and 80 °C. The cross symbols express the polarizing azimuths of the polarizer and analyzer. The x, y, and z directions correspond to those in Fig. 1. The insets show p- and s-polarization components of transmittance spectra at incident and transmission angles of 0° at temperatures below and above T_{NI} for the respective samples.

as follows:

$$n_e(\lambda) = 1.667\,65 + 0.012\,21\lambda^{-2} + 0.001\,54\lambda^{-4} \quad \text{and} \quad (13)$$

$$n_o(\lambda) = 1.493\,31 + 0.008\,68\lambda^{-2} - 0.000\,27\lambda^{-4}. \quad (14)$$

In the same way, the refractive indices of K15 at 20 °C are expressed as

$$n_e(\lambda) = 1.663\,99 + 0.016\,60\lambda^{-2} + 0.001\,79\lambda^{-4} \quad \text{and} \quad (15)$$

$$n_o(\lambda) = 1.494\,39 + 0.016\,41\lambda^{-2} - 0.000\,50\lambda^{-4}. \quad (16)$$

The refractive indices n_{ply}, n_e, and n_o are shown together with the Cauchy's dispersion curves as a function of wavelength in Figs. 4(a) and 4(b) for BL024 and K15, respectively. The values of n_e and n_o for the LC materials agree with the literature values [29–31], which are shown as crosses in the figures. Furthermore, the values for isotropic states, n_i, are plotted, which were measured at and above T_{NI}.

B. Diffraction spectra and structural identification

Two groups of HPDLC samples were investigated, as tabulated in Table I. Samples I–III were fabricated at different exposure temperatures using the same material composition as the starting mixture, such that the variations of LC droplet shape and distribution in the same polymer matrix was expected to quantitatively examine the relationship between the optical anisotropy and phase-separation morphology. Samples IV–VI formed periodic structures at various compositional ratios in starting mixture, which allowed us to examine the influence of the filling volume of LC droplets in polymer matrix on diffraction properties.

Six independent Bragg diffraction spectra were measured at p- and s-polarized states at temperatures below, at, and above T_{NI}. To determine the structural parameters a, b, β, and S, the six spectra were consistently fitted all at once to Eqs. (1) and (2) under the restraints imposed by Eqs. (3)–(11), assigning Eqs. (12)–(14) for samples I–III and Eqs. (12), (15), and (16) for samples IV–VI.

Figures 5(a) and 5(b) show the diffraction spectra of samples I and III, which were fabricated at exposure temperatures of 30 °C and 80 °C, respectively. For the case at an exposure temperature of 30 °C, as shown in Fig. 5(a), in the nematic phase at temperatures below T_{NI} (the blue solid and open circles), the p-polarized light was preferentially diffracted; in other words, $\eta_p > \eta_s$. When the exposure temperature was increased, η_p decreased, as shown in Fig. 5(b). On the other hand, at temperatures above T_{NI}, the values η_p and η_s approached each other as the LC phase changed toward isotropy, as shown by the green triangles and red rectangles, respectively. However, η_p does not completely agree with η_s even at temperature above T_{NI}, and the deviation between η_p and η_s, as shown by red solid and open circles, respectively, tends to be larger at lower exposure temperatures.

Six diffraction spectra for the p and s components at temperatures below, at, and above T_{NI} were simultaneously fitted to Eqs. (1) and (2) under the restraints imposed by Eqs. (3)–(11), where Eqs. (12)–(14) were substituted for n_{ply}, n_e, and n_o, respectively, as indicated by the solid and broken curves in blue circles, green triangles, and red rectangles, respectively, in Fig. 5. The wavelength dispersions of anisotropic refractive indices for the respective phases, n_{1x}, n_{1yz}, n_{2x}, and n_{2yz} were obtained by the curve fitting, as shown in the insets in Fig. 5. The determined structural parameters a, b, β, and S by the curve fittings were plotted as functions of the exposure temperature (Fig. 6). The filling ratios of the LC droplets, a and b, were approximately 0.3 and 0, respectively, and they were mostly constant as a function of the exposure temperature. The filling ratios in this system indicate that the LC droplets strongly tend to gather locally to form a LC-rich phase, whereas no LC droplet exists in a polymer-rich phase or it can be regarded as fully polymer phase. The orientational order parameter for LC molecules in the droplets, S, below T_{NI} does not significantly change at about 0.5 as the exposure temperature varied. On the other hand, S at a temperature of T_{NI} drastically changes against exposure temperature, and at a temperature above T_{NI} it remains more than zero. The thermo-optic coefficient in LC droplets, β, remained constant at -0.27×10^{-3} (K^{-1}) at any exposure temperature and is

larger than the value for LC raw material, as expressed by the broken line, which was pre-examined from the results as shown in Fig. 4(a).

Figures 7(a) and 7(b) show the diffraction spectra of samples IV and VI, which were fabricated from different ratios of LC in the starting material. At temperatures below T_{NI}, the diffraction efficiency for the low compositional ratio of LC is similar to that for the high one in the present system, as shown by a comparison of the blue solid and open circles in Fig. 7(a) with those in Fig. 7(b). The solid and broken curves for blue circles, green triangles, and red rectangles are the curve fittings to Eqs. (1) and (2) under the restraints imposed by Eqs. (3)–(11), where Eqs. (12), (15), and (16) were substituted for n_{ply}, n_e, and n_o, respectively. The wavelength dispersions of n_{1x}, n_{1yz}, n_{2x}, and n_{2yz} obtained by the curve fittings are shown in the insets in Fig. 7. The refractive indices in the inset in Fig. 7(a) are quite different from those in Fig. 7(b), even though the diffraction data at temperatures below T_{NI} were similar to each other. The results of $n_{1x} \neq n_{1yz}$ and $n_{2x} = n_{2yz}$ at 20 °C in the inset in Fig. 7(a) suggest that the LC-rich phase is anisotropic and the polymer-rich one is isotropic. On the other hand, the results of $n_{1x} \neq n_{1yz}$ and $n_{2x} \neq n_{2yz}$ at 20 °C in the inset in Fig. 7(b) suggest that both LC- and polymer-rich phases are anisotropic. The structural parameters a, b, β, and S, determined by the curve fittings, were plotted as functions of the concentration of the LC starting material (Fig. 8). As the concentration of the LC material increased from 40% to 50%, the filling ratio of LC droplets in the LC-rich phase, a, increased from 0.5 to 0.75. In contrast, the filling ratio of the LC droplets in the polymer-rich phase, b, remained at 0 for LC concentrations less than 45% and began to increase when the LC concentration increased beyond 45%. The result of $b > 0$ indicates that LC molecules exist in the polymer-rich phase. The molecular orientational order in the LC droplets, S, below T_{NI} gradually increased from 0.9 to 1 with the increase in LC concentration, whereas S at and above T_{NI} is mostly zero. The thermo-optic coefficient of the LC molecules in the droplets, β, decreased from -0.5×10^{-3} to -0.7×10^{-3} (K^{-1}) with the increase in LC ratio, and they deviate smaller from the original value as expressed by the broken line.

Diffraction may appear at the Bragg's conditions for grating pitches of not only Λ but also $\Lambda/2$, $\Lambda/3$, . . ., dependently on sample preparation condition. Figures 9(a) and 9(b) for samples IV and VI, respectively, show the intensity, wavelength, and incident angle of all the Bragg diffractions detected here in the p-polarization state at 20 °C. The upper graphs show the relationship between wavelength and incident angle where the Bragg diffraction was detected as shown in

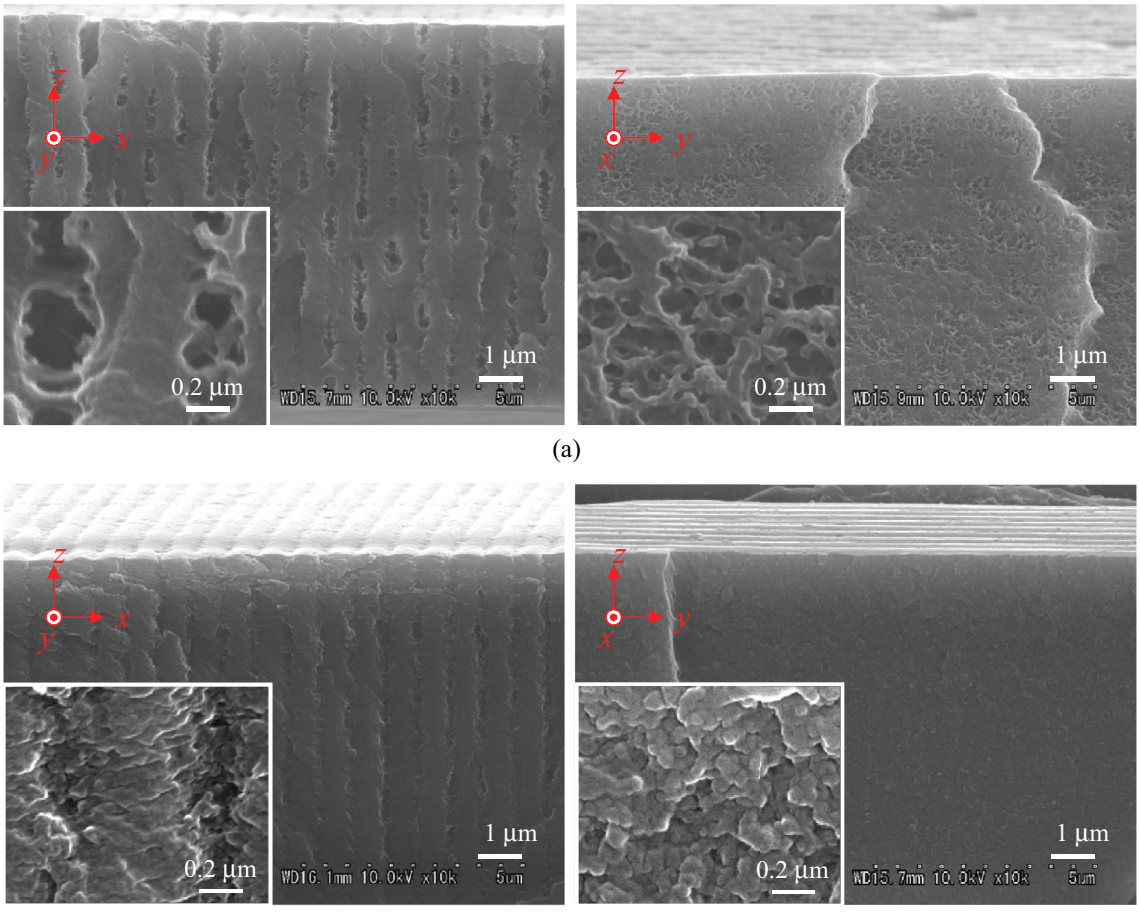

FIG. 11. (Color online) The x-z and y-z cross sections observed by SEM for (a) sample I and (b) sample III, corresponding to those in Fig. 10, where the x, y, and z directions correspond to those in Fig. 1. The insets show close-up views.

the lower graphs. Note that θ_B' is the angle in HPDLC media, estimated by Snell's law. The solid curves are the estimations of the Bragg formula modified on the assumption of Λ/N in grating pitch, as indicated in the graphs, where $N = 1, 2, \ldots$. The data can be classified into $N = 1, 2, \ldots$, as expressed by different symbols approximately on the respective curves, and thus the detected diffractions as shown in the lower graphs may be regarded as the Bragg ones for Λ/N in grating pitch, where the data for $N = 1$ in Fig. 9 were brought from the ones in Fig. 7. The diffraction spectra for $N \geqslant 2$ in Fig. 9(b) are depressed rather than those in Fig. 9(a). This result suggests that the refractive index is sinusoidally modulated at a picth of Λ in the HPDLC for sample VI as compared with that for sample IV.

V. DISCUSSION

The present analysis method was examined in validity by comparisons of the analyzed structures in diffractometry with direct images in microscopic observations. In the present study, the structures were observed along x, y, and z axes by using SEM or POM. Figures 10(a) and 10(b) show the transmission micrographs of the x-y plane observed by POM in a crossed Nicol state for samples I and III, respectively. The bright regions indicate high optical anisotropy, whereas the dark regions indicate low optical anisotropy. The samples contained a one-dimensional periodic structure consisting of high- and low-anisotropic phases. The more anisotropic area (the higher-contrast part) most likely corresponds to the LC-rich phase, in which the orientation of LC molecules was highly ordered along the x axis, while the less anisotropic area (the low-contrast part) is regarded as the polymer-rich phase. Sample I, which was formed by holographic exposure at 30 °C, showed inhomogeneous optical anisotropy, in addition to the regular periodicity [Fig. 10(a)]. Such additional inhomogeneity was suppressed with the increase in the exposure temperature [Fig. 10(b)]. The behaviors of transmittance spectra against polarization and temperature are shown in the insets, where the incident and transmission angles were set at 0°. It suggests that the anisotropic inhomogeneity produces light scattering particular in p polarization and it is due to the orientation of LC molecules.

The SEM images of the periodic structures in the x-z- and y-z-plane cross sections for samples I and III in Figs. 11(a) and 11(b), respectively, show the distribution of voids in the polymer matrix, which was left after the LC droplets were rinsed away with methanol. The voids appearing in x-z cross sections show that the LC droplets locally aggregated to form LC-rich layers, and no droplet was observed in polymer-rich layers. This result agrees with the structural parameters of $a > 0$ and $b = 0$ for samples I–III, as stated in Sec. IV with Fig. 6. The size and shape of the LC droplets depend on the exposure temperature. The x-z cross section of sample I, in which the exposure temperature was 30 °C, contained LC droplets at a few hundred nanometers in size, as shown in Fig. 11(a). The networklike cross-linking of the polymer or the coalescence of the droplets perpendicular to grating vector in LC-rich phase, as shown by the y-z cross section in Fig. 11(a), suggests that the droplets aggregated on a submicrometer scale probably produced the inhomogeneous optical anisotropy and consequent light scattering shown in Fig. 10(a). The smaller droplets appearing in sample III, in which the exposure temperature was 80 °C, were distributed more homogeneously along the y-z plane than those in sample I. This homogeneous distribution is considered to have created the regular periodic distribution with optical anisotropy shown in Fig. 10(b). Such anisotropic distribution and coalescence of LC droplets along the y-z plane are speculated to regularize LC orientation along the grating vector (z axis).

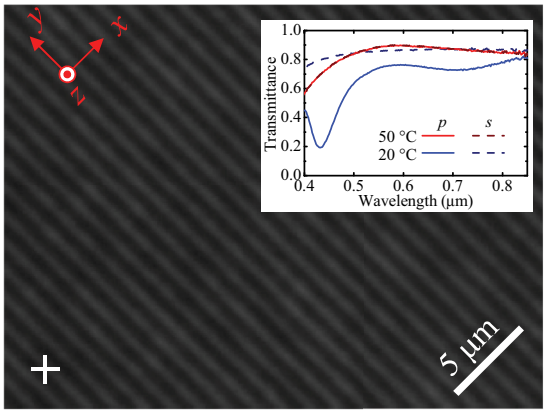

(a)

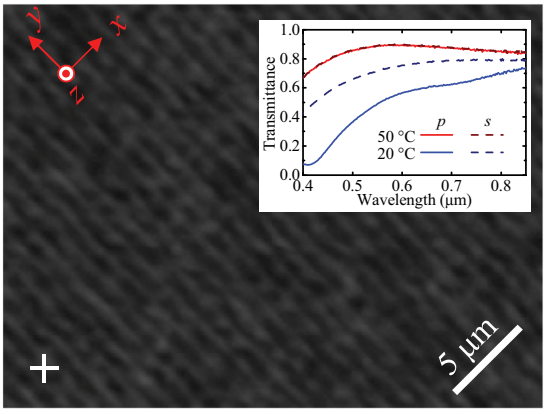

(b)

FIG. 12. (Color online) HPDLC transmission images of samples formed using different compositions, observed by POM in a crossed Nicol state at 20 °C: (a) sample IV with 40 wt% LC and (b) sample VI with 50 wt% LC. The cross symbols express the polarizing azimuths of polarizer and analyzer. The x, y, and z directions correspond to those in Fig. 1. The insets show p and s polarization components of transmittance spectra at incident and transmission angles of 0° at temperatures below and above T_{NI} for the respective samples. Note that the valley at around 0.43 μm in wavelength is regarded to be due to Raman-Nath diffraction in Fig. 12(a).

Figures 12(a) and 12(b) show the transmission micrographs of the x-y plane observed by POM in a crossed Nicol state for samples IV and VI, respectively. At a low compositional ratio of LC material, a distinct periodic contrast was observed, as shown in Fig. 12(a), whereas at a high ratio, the periodic contrast was disturbed by the additional domains, as shown in Fig. 12(b). This additional inhomogeneity may produce light scattering, as shown in the insets. The cross-sectional images of the periodic structure observed by SEM, shown in Fig. 13,

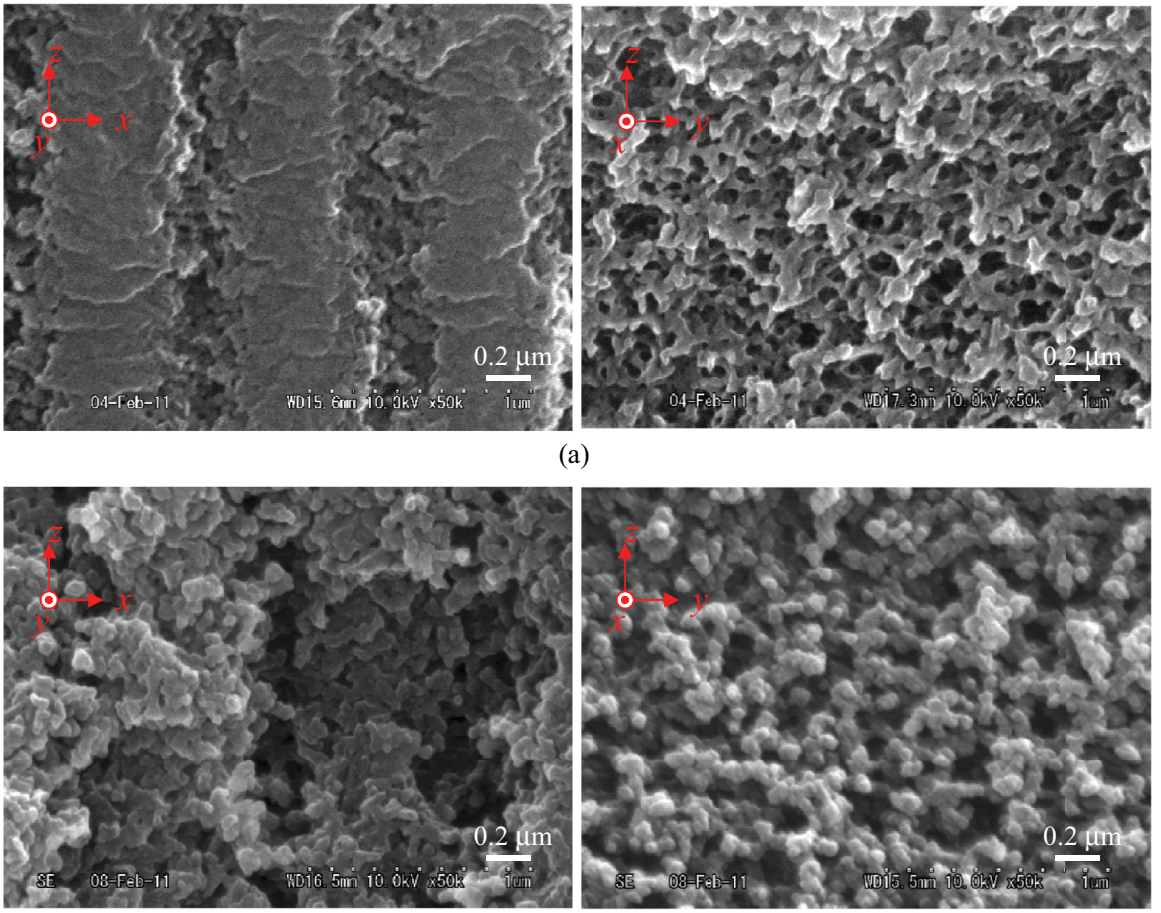

FIG. 13. (Color online) The x-z and y-z cross sections observed by SEM for (a) sample IV and (b) sample VI, corresponding to those in Fig. 12, where the x, y, and z directions correspond to those in Fig. 1.

were qualitatively consistent with the POM contrast images shown in Fig. 12. At a low ratio of LC material [Fig. 13(a)], LC- and polymer-rich phases formed distinct periodic structures. In particular, the polymer component fully occupied to form polymer phase, whereas the majority of LC droplets were gathered in the LC-rich phase. On the other hand, as the ratio of LC material increased, the boundary between the LC- and polymer-rich phases became unclear [Fig. 13(b)]. The LC droplets encroached on the polymer-rich phase; in other words, the polymer domains were dispersed in the LC phase. This result is expressed by the filling ratio of LC, a, b, as stated in Sec. III with Fig. 8; that is, b discretely changes from zero to nonzero with the increase in compositional ratio of LC, while a keeps nonzero and simply increases.

The validity of LC occupations in LC- and polymer-rich phases, a and b, are evaluated by examining the deviation of the average LC occupation in the HPDLC, $(a+b)/2$, with LC ratio in the starting material mixtures as listed in Table I. The values of $(a+b)/2$ for samples I to III, 0.14–0.17, as shown in Fig. 6, are approximately 0.1 smaller than the LC ratio of the starting mixtures, which was set at 0.25 constant. The same tendency was found for samples IV and V; that is, the values of $(a+b)/2$ are 0.24 and 0.27, and they are roughly 0.2 smaller than the LC ratio of the starting mixtures, 0.40 and 0.45, respectively. On the other hand, the value for sample VI, 0.54, mostly agrees with the LC ratio in the starting mixture, 0.5. As a microscopic origin of the deviation of $(a+b)/2$ from the estimated LC ratio, the dissimilarity of practical refractive-index modulation from sinusoidal function is speculated, which is derived from the comparison of the results between samples IV and VI, as shown in Fig. 9. Accordingly, the present deviation of $(a+b)/2$ from the LC ratio in sample preparations may be possibly due to the diffraction analysis with Eqs. (1) and (2) assuming sinusoidal modulation in refractive index for the practical samples.

It was found that the LC orientation order parameter, S, may remain more than zero at temperatures even above T_{NI}, as shown in Fig. 6. Since such behaviors of S varies with exposure temperature even for the samples fabricated from the same starting mixture, LC molecular orientation is speculated to be affected morphologically by size, shape, and arrangement of LC droplets through a kind of anchoring effect on the boundaries between the LC droplets and the polymer matrix surrounding them, although the further evidence to support this speculation may be indispensable.

VI. CONCLUSIONS

A widely useful optical diffractometry method was proposed for quantitative analysis of the microscopic structural

origins of a highly polarized diffraction grating produced by holographic HPDLCs, which were formed through photoinduced inhomogeneous polymerization and subsequent phase separation into polymer and LC phases. The present method was demonstrated for two types of characteristic samples with regard to the phase-separation morphology and the filling ratio of LC to polymer and then was examined in validity by comparison with microscopic observations with polarizing microscopy and SEM.

As an unconventional process in the present diffractometry, six independent Bragg diffraction spectra were measured in two orthogonal polarization states at temperatures below, at, and above the nematic-to-isotropic phase transition point. Then the spectra were consistently analyzed all at once by employing anisotropic diffraction theory under the restraints of a simple but consistent structural model, such as the filling ratio of LC droplets to polymer matrix, the molecular orientational order in LC droplets and the thermo-optic properties of the LC molecules in the droplets. The present analysis found that the LC orientation strongly contributes to the polarization state in the diffraction, and in some cases, it remains ordered even at temperatures above the nematic-to-isotropic phase transition point. Furthermore, the higher order Bragg diffractions were detected to discuss more detail about the spatial distribution of the refractive index in the HPDLCs. The present analysis method with spectroscopic diffractometry displayed great potential to obtain significant and quantitative information in various microscopic structures of HPDLCs.

ACKNOWLEDGMENTS

This work was supported in part by a JSPS Grant-in-Aid for Scientific Research C (23560427).

[1] A. Urbas, J. Klosterman, V. Tondiglia, L. Natarajan, R. Sutherland, O. Tsutsumi, T. Ikeda, and T. Bunning, Adv. Mater. **16**, 1453 (2004).
[2] M. J. Escuti, J. Qi, and G. P. Crawford, Opt. Lett. **28**, 522 (2003).
[3] R. Jakubiak, T. J. Bunning, R. A. Vaia, L. V. Natarajan, and V. P. Tondiglia, Adv. Mater. **15**, 241 (2003).
[4] K. Yoshino, Y. Shimoda, Y. Kawagishi, K. Nakayama, and M. Ozaki, Appl. Phys. Lett. **75**, 932 (1999).
[5] H. Kakiuchida, M. Tazawa, K. Yoshimura, and A. Ogiwara, Sol. Energy Mater. Sol. Cells **94**, 1747 (2010).
[6] M. Sarkar, N. L. Gill, J. B. Whitehead, and G. P. Crawford, Macromolecules **36**, 630 (2003).
[7] E. H. Jeong, J. Y. Woo, Y. H. Cho, Y. K. Jeong, K. H. Kima, and B. K. Kim, Polym. Int. **58**, 171 (2009).
[8] S.-T. Wu, T.-S. Mo, A. Y.-G. Fuh, S.-T. Wu, and L.-C. Chien, Jpn. J. Appl. Phys. **40**, 6441 (2001).
[9] A. Ogiwara, H. Kakiuchida, M. Tazawa, and H. Ono, Jpn. J. Appl. Phys. **46**, 7341 (2007).
[10] A. Ogiwara, M. Minato, S. Horiguchi, H. Ono, H. Imai, H. Kakiuchida, and K. Yoshimura, Jpn. J. Appl. Phys. **47**, 6688 (2008).
[11] H. Kogelnik, Bell Sys. Tech. J. **48**, 2909 (1969).
[12] G. Montemezzani and M. Zgonik, Phys. Rev. E **55**, 1035 (1997).
[13] J. J. Butler and M. S. Malcuit, Opt. Lett. **25**, 420 (2000).
[14] J. J. Butler, M. S. Malcuit, and M. A. Rodriguez, J. Opt. Soc. Am. B **19**, 183 (2002).
[15] M. E. Holmes and M. S. Malcuit, Phys. Rev. E **65**, 066603 (2002).
[16] M. Jazbinšek, I. D. Olenik, M. Zgonik, A. K. Fontecchio, and G. P. Crawford, J. Appl. Phys. **90**, 3831 (2001).
[17] I. Drevenšek-Olenik, M. Jazbinšek, M. E. Sousa, A. K. Fontecchio, G. P. Crawford, and M. Čopič, Phys. Rev. E **69**, 051703 (2004).
[18] I. Drevenšek-Olenik, M. Fally, and M. A. Ellabban, Phys. Rev. E **74**, 021707 (2006).
[19] D. E. Lucchetta, L. Criante, and F. Simoni, Opt. Lett. **28**, 725 (2003).
[20] E. H. Kim, J. Y. Woo, and B. K. Kim, Displays **29**, 482 (2008).
[21] J. Y. Woo, E. H. Kim, S. S. Shim, and B. K. Kim, Opt. Commun. **281**, 2167 (2008).
[22] M. Mucha, Prog. Polym. Sci. **28**, 837 (2003).
[23] A. Ogiwara, S. Horiguchi, H. Kakiuchida, M. Tazawa, K. Yoshimura, and H. Ono, Opt. Lett. **33**, 1521 (2008).
[24] S. Meng, T. Kyu, L. V. Natarajan, V. P. Tondiglia, R. L. Sutherland, and T. J. Bunning, Macromolecules **38**, 4844 (2005).
[25] R. R. Deshmukh and M. K. Malik, J. Appl. Polym. Sci. **109**, 627 (2008).
[26] T. Chen, L. Zhang, T. Li, J. Lin, and S. Lin, J. Polym. Sci. **B45**, 1898 (2007).
[27] F. Basile, F. Bloisi, L. Vicari, and F. Simoni, Phys. Rev. E **48**, 432 (1993).
[28] L. Vicari, J. Appl. Phys. **81**, 6612 (1997).
[29] R. Yamaguchi and S. Sato, IEICE Trans. CJ **71-C**, 1241 (1988) [in Japanese].
[30] I. Chirtoc, M. Chirtoc, C. Glorieux, and J. Thoen, Liq. Cryst. **31**, 229 (2004).
[31] Product catalogue of Merck KGaA.